

# Global Interdependencies between Economic Policy Uncertainty and Geopolitical Risk Indices

March 5, 2025

## Abstract

We study the complex interdependencies between global newspaper-based economic policy uncertainty (EPU) and geopolitical risk (GPR) indices. We investigate monthly EPU and GPR series for 20 countries between January 1997 and December 2024. We employ the Complex Hilbert Principal Component Analysis (CHPCA) to understand the importance of lead-lag relationships and the mutual influences of global EPU and GPR indices. We investigate the weighted and directed networks using complex correlation matrices to extract the magnitude and phase of the indices, indicating significance and leading role. Our findings suggest that, among others, the terrorist attack of September 11, 2001, and the Russia - Ukraine conflict in 2022 are the most notable EPU or GPR events during the sample period. The results show that, based on the Helmholtz-Hodge (HH) potential, most notably, China's EPU affects the GPRs of Egypt and Israel, and Russia's EPU influences the GPRs of Taiwan, Japan, and China.

**keywords:** Complex Interdependencies; Economic Policy Uncertainty (EPU); Geopolitical Risk (GPR); Complex Hilbert Principal Component Analysis (CHPCA); Helmholtz-Hodge (HH) Decomposition

**classcode:** C38, F62, G18

# 1 Introduction

This paper investigates the complex interdependencies between newspaper-based economic policy uncertainty (EPU) and geopolitical risk (GPR) indices worldwide to identify their leading and lagging relationships and their effects on each other. As uncertainty is related to risk, it can affect the economy by reducing economic activity or increasing unemployment (Bernanke, 1983; Bloom, 2009).

In this study, we propose a comprehensive analysis of the relationships between EPU and GPR indices at a global level since economic and financial systems are connected beyond countries' borders, as evidenced by events such as the 2008 Global Financial Crisis (GFC) or the 2022 Russian invasion of Ukraine. We analyze the complex interconnectedness or leading and lagging relationships between EPU and GPR indices using a novel Complex Hilbert Principal Component Analysis (CHPCA) methodology, operating in the complex realm and well suited to capture the leading and lagging relationships of the EPUs and GPRs. The rotational random shuffling (RRS) method (see Vodenska *et al.* (2016)) enables us to separate the data relationships into the signal (principal) and noise components. We construct the pseudo-correlation matrix using only the principal components and call this matrix the principal correlation matrix. Since the components of the principal correlation matrix are complex numbers, we can represent them in terms of amplitude and phase. Hence, we can understand the complex correlation matrix as a composite of amplitude and phase correlation matrices. The amplitude correlation matrix yields a weighted and undirected network. We obtain a directed network by applying the Helmholtz-Hodge (HH) decomposition to the phase correlation matrix to identify leading and lagging relations of the EPU and GPR indices. We consider the leading index a source and the lagging index a sink.

We build our study on policy-related economic uncertainty research, including Baker *et al.* (2016), who proposed the EPU measure based on media coverage of specific events related to economic uncertainty. The EPU is constructed by counting articles containing the terms “uncertain” or “uncertainty”, “economic,” or “economy,” and one or more policy-relevant newspaper terms. Using the Vector Autoregressive (VAR) framework, the authors show that increases in EPU have non-negligible repercussions on the global economy. Moreover, Caggiano *et al.* (2020) point out that economic policy uncertainty is relevant and can be one of the key drivers of changes in actual economic activity in the United States (US), confirming previous findings (Bloom, 2017; Castelnovo *et al.*, 2017). King and Wadhvani (1990) have used contagion root analysis to study global information transmission, where rational agents seek to infer information from price behavior in other stock markets.

Using a similar automated text-search procedure, Caldara and Iacoviello (2022) propose the geopolitical risk (GPR) index, which represents the “*threat, realization, and escalation of adverse events associated with wars, terrorism, and any tensions among states and political actors that affect the peaceful course of international relations*” (Caldara and Iacoviello, 2022, p. 1195). The study states that GPRs are regarded by entrepreneurs, market participants, and central bankers as key variables that affect investment decisions and stock market behavior. Additionally, they report that the GPR measures a different source of risk compared to the EPU

and the VIX indices, displaying a sizable amount of non-common variability. The GPR is based on the share of articles referring to adverse geopolitical events, such as wars and terror attacks. A common underlying characteristic of the EPU and the GPR indices is that these measures are constructed from newspaper-based articles. Both indices are available monthly, allowing for a higher resolution of economic uncertainty indicators than quarterly or annual macroeconomic measures.

To increase the valuable contributions of these two indices, given their importance to market participants, one natural extension is to study their interdependencies across countries and regions using a novel methodology. Researchers have used the CHPCA method to study biennial variations in surface temperatures (Rasmusson *et al.*, 1981), complex principal component analysis (Horel, 1984), dynamic correlations in financial markets (Arai *et al.*, 2013), interdependencies in coupled financial networks of equity and foreign exchange markets (Vodenska *et al.*, 2016), economic network synchronizations (Aoyama *et al.*, 2017), and relationships between macroeconomic indicators and business cycles (Iyetomi *et al.*, 2020).

Our research also builds on findings by Klößner and Sekkel (2014), who investigate a potential transmission of economic policy uncertainty among six developed economies: Canada, France, Germany, Italy, the United Kingdom, and the US. They study fluctuations in policy uncertainty in one country and their effects on policy uncertainty in other countries to understand which economies are net uncertainty exporters or importers. They use a sample from January 1997 to September 2013 to employ the spillover index methodology from Diebold and Yilmaz (2009). Klößner and Sekkel (2014) study finds evidence that over 25% of the countries' EPU behavior is due to spillovers across economies in the sample they study. They find that the U.S., followed by the United Kingdom, is the highest net exporter of uncertainty, and Italy shows the most independent fluctuation. During the financial crisis, their analyses show that the spillover index increased.

Balli *et al.* (2017) extend the results of Klößner and Sekkel (2014) by providing evidence on the spillovers of policy uncertainty across 16 countries and go further by exploring the cross-sectional determinants of these pairwise effects using Diebold and Yilmaz (2012)'s methodology. The results imply that the U.S., Australia, and Canada (US, Australia and Italy) contribute the most to the mean (volatility) spillover, and variables such as bilateral trade and common language are related to the transmission of net policy uncertainty between countries. Kang and Yoon (2019) apply the Diebold and Yilmaz (2014, 2015) spillover approach to the EPU indices of 9 countries and document a high level of policy-induced uncertainty interconnection among them. The total spillover index is above 65% on average, with the EU being the most influential as a net transmitter of policy uncertainty. In addition, their findings highlight the role played by China during the 2008 GFC and the European sovereign debt crisis in 2012, becoming one of the largest net exporters of policy uncertainty spillovers. This finding is also supported by Liow *et al.* (2018), who show that China was a source of policy uncertainty spillover to other economies during the GFC. Marfatia *et al.* (2020) and Yang *et al.* (2021) use the network theory approach to provide evidence of interconnection between global EPUs.

Concerning geopolitical risk transmission shocks, we build on Balli *et al.* (2022), one of the few research studies on the subject close to ours. Using the Diebold and Yilmaz (2012) spillover measure and Baruník and Křehlík (2018) methodology, the authors identify short- and long-term GPR transmissions between January 1985 and December 2016. They focus on understanding how different countries' GPRs are transmitted and employ a gravity model to explain these features. Balli *et al.* (2022) point out a non-negligible level of connectedness. The study reports a total mean spillover of over 39% among the 19 countries in their sample, with larger countries associated with higher GPR transmission. The closer the countries are, the higher the spillover among them. There is also evidence that variables such as bilateral trade, border sharing, and the distance between countries are relevant in determining pairwise GPR propagation in the overall analysis. Finally, the total short-term GPR transmission (up to 3 months) is larger than that for the long-term (3-100 months), 32% and 7%, respectively.

The contribution of our study is three-fold. First, the paper contributes to the study of integrated markets, uncovering the interconnectedness between countries to capture early warning signals to avoid disseminating policy uncertainty, geopolitical tensions, or financial crises. Second, it highlights the EPU and GPR transmission dynamics between larger and smaller economies. Third, it could aid investors in portfolio diversification decisions through an improved understanding of the dynamics between countries and their mutual EPU and GPR influence.

The remainder of this paper is organized as follows. Section 2 describes the data, Section 3 explains the methodology, Section 4 presents our findings, and Section 5 concludes.

## 2 Data

We obtained the EPU and GPR indices between January 1997 and December 2024 from the Economic Policy Uncertainty website EPU (2025). In this section, we explain the dataset's details and the index selection to study a broad sample of countries.

### 2.1 Economic Policy Uncertainty (EPU)

The EPU has been measured for the U.S., Canada, Ireland, and Sweden since 1985. However, for the broader set of countries we study in this paper, the EPU has been available since 1997. The number of newspapers used to construct the index varies between countries; for instance, in Brazil, only one newspaper is used, while in the U.S., 10 newspapers are used for calculating the EPU index. All country-level data contains information on global versions of the EPU and 23 country-level EPUs, i.e., GEPU\_current, GEPU\_ppp, Australia, Brazil, Canada, Chile, China (Mainland China, Hybrid China, and SCMP China), France, Germany, Greece, India, Ireland, Italy, Japan, Korea, Pakistan, Russia, Spain, Singapore, the UK, the U.S., Sweden, and Mexico.

Since we are interested in the leading and lagging relationships of the EPU indices between countries, we

exclude the GEPU\_current and the GEPU\_ppp indices. According to EPU (2025), “*the GEPU Index is a GDP-weighted average of national EPU indices for 21 countries: Australia, Brazil, Canada, Chile, China, Colombia, France, Germany, Greece, India, Ireland, Italy, Japan, Mexico, the Netherlands, Russia, South Korea, Spain, Sweden, the United Kingdom, and the United States.*” There are “*two versions of the GEPU Index - one based on current-price GDP measures, and one based on PPP-adjusted GDP.*”

As explained in EPU (2025), “*a hybrid index is an average of two indices, one based on the South China Morning Post and another based on Mainland China newspapers.*” Both indices follow the newspaper approach of Baker *et al.* (2016); the former relies on the South China Morning Post (SCMP), Hong Kong’s leading English-language newspaper, while the latter uses two mainland Chinese newspapers: the Renmin Daily and the Guangming Daily. The SCMP China is unavailable after December 2023, therefore we use the EPU of mainland China as the EPU-CHN.

We choose 16 countries for the EPU indexes. Their ISO 3166-1 alpha-3 codes are: AUS, BRA, CAN, CHL, FRA, DEU, GRE, IND, ITA, JPN, KOR, RUS, ESP, GBR, USA, CHN. The heat map of the annual average of EPU normalized by the highest value of each index is shown in the top 16 rows in Figure. 1. The appendix shows the original countries’ monthly time series of the EPU indices.

## 2.2 Geopolitical Risk (GPR) index

We obtained the GPR indices between January 1997 and August 2024 from the Economic Policy Uncertainty website EPU (2025). The country-specific GPR refers to the share of articles mentioning geopolitical terms. The GPR index is based on leading English-language newspapers, and there are two versions of the index: historical GPR since 1900 and country GPR (GPRC), which is available for 44 countries since 1985. In our study, we use the GPRC from January 1997 to December 2024. From the 44 available GPR indices, we select 19 countries to include in our study. Their ISO 3166-1 alpha-3 codes are AUS, BRA, CAN, CHL, CHN, FRA, DEU, IND, ITA, JPN, KOR, RUS, ESP, GBR, USA, EGY, ISR, TWN, and UKR. The heat map of the annual average of the GPRs normalized by the highest value of each index is shown as the 19 bottom rows in Figure. 1. The appendix shows the original monthly time series of the GPR indices.

## 2.3 Time evolution of EPUs and GPRs

The EPU and GPR indices have shown different dynamics between 1997 and 2024, generally exhibiting higher values toward the end of the study period. Figure. 1 represents the heat map of the annual averages of the EPU and the GPR indices, normalized by the largest value of each index. We observe that the more recent years, characterized by higher EPUs and GPRs, are dominated by the U.S.-China economic frictions, the COVID-19 pandemic, the energy crisis-driven inflation due to the Russian invasion of Ukraine, and the Israeli-Hamas war. Earlier in the late 1990s and early 2000s, we observe the Japanese financial crisis, the September 11 attacks,

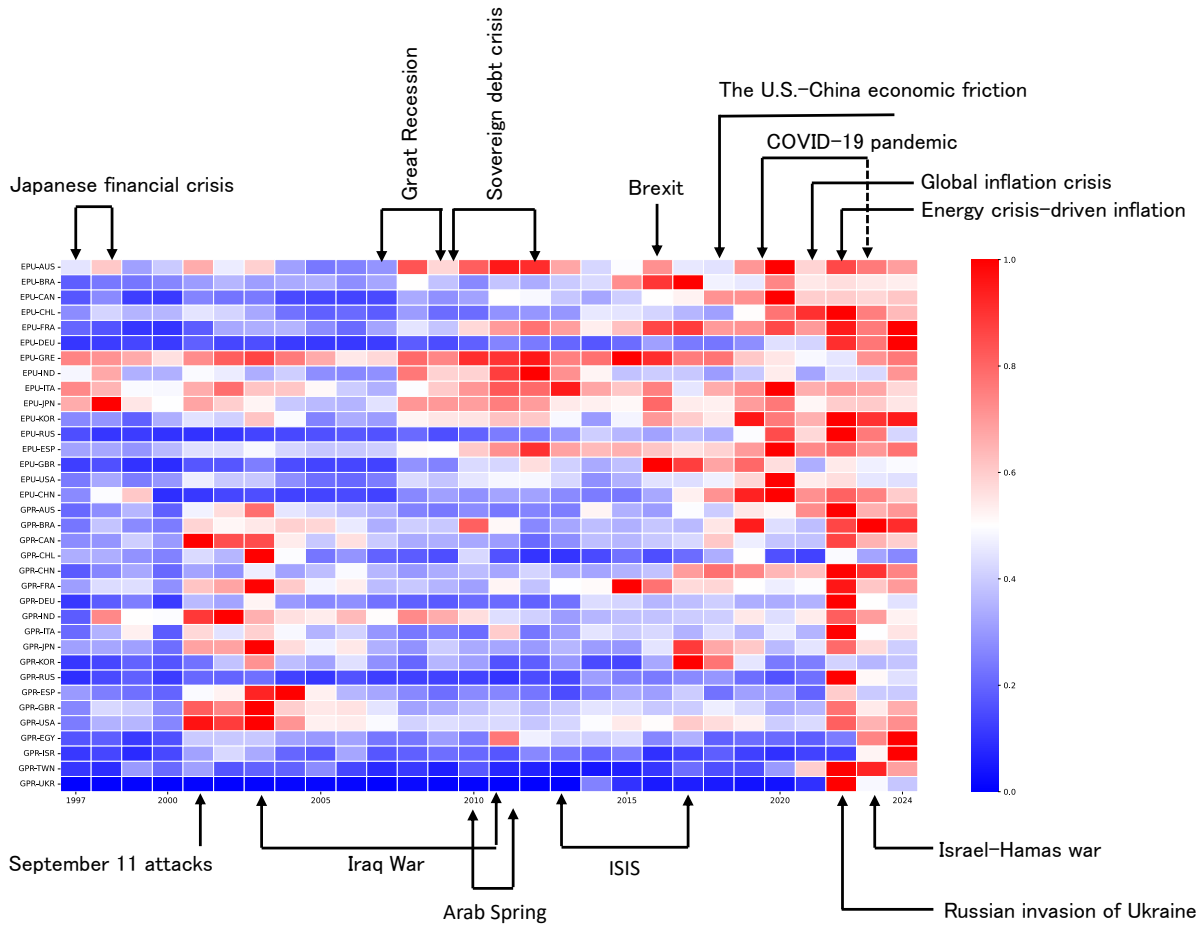


Figure 1: Heat map of the yearly average of EPU and GPR indices, normalized by the largest value of each index. The horizontal direction shows the years from 1997 to 2024, and the vertical direction depicts the order of the countries. The upper part from Australia (EPU-AUS) to mainland China (EPU-CHN) (16 countries) corresponds to the EPUs. The lower part from Australia (GPR-AUS) to Ukraine (GPR-UKR) (19 countries) corresponds to the GPRs. This figure also includes some of the major historical EPU and GPR events.

and the Iraq War, followed by the Global Financial Crisis (GFC) of 2008 and the European Sovereign Debt crisis in 2012. Collectively, these events dominate the world’s EPU and GPR landscape.

### 3 Methods and Materials

This section explains the complex Hilbert PCA (CHPCA) to explore the correlation structure of global EPU and GPR indices. The study investigates the global leading and lagging relationships among the EPUs of 16 and the GPRs of 19 countries from January 1997 to December 2024, i.e., 35 time series, each with 336 monthly observations.

### 3.1 Complex correlation matrix

We denote time series data of  $n$ -th component at time  $t$  as  $x_{n,t}$ . Here,  $n$  corresponds to the EPU and GPR combined with ISO 3166-1 alpha-3 codes, i.e., {EPU-AUS, ..., EPU-CHN, GPR-AUS, ..., GPR-UKR}, as shown in Figure. 1. Some of the original time series of EPU and GPR are non-stationary processes and contain a value of 0. Therefore, to convert non-stationary processes containing a value of 0 to stationary processes, we adopt the first-order difference of the time series defined as follows:

$$r_{n,t} = x_{n,t} - x_{n,t-1} , \quad (1)$$

where  $n = 1, \dots, N$  and  $t = 1, \dots, T$ . In this paper,  $N = 35$  and  $T = 336$ . The mean value of the first-order difference is defined as follows:

$$\langle r_n \rangle = \frac{1}{T} \sum_{t=1}^T r_{n,t} , \quad (2)$$

and its variance is defined as follows:

$$\sigma_n^2 = \frac{1}{T-1} \sum_{t=0}^T (r_{n,t} - \langle r_n \rangle)^2 . \quad (3)$$

We standardize the first-order difference defined by Equation (1) to have a mean value equal to zero and a variance equal to one:

$$w_{n,t} = \frac{r_{n,t} - \langle r_n \rangle}{\sigma_n} . \quad (4)$$

After the standardization, all-time series  $w_n$  passed the Augmented Dickey-Fuller (ADF) test and Kwiatkowski-Phillips-Schmidt-Shin (KPSS) test for stationarity.

We then perform the Fourier transform of Equation (4) as follows:

$$w_{n,t} = \sum_{k=0}^T [a_n(\omega_k) \cos(\omega_k t) + b_n(\omega_k) \sin(\omega_k t)] , \quad (5)$$

where  $\omega_k = 2\pi k/T \geq 0$ . The Hilbert transform of Equation (5) is given by:

$$\hat{w}_{n,t} = \sum_{k=0}^T [b_n(\omega_k) \cos(\omega_k t) - a_n(\omega_k) \sin(\omega_k t)] . \quad (6)$$

Equation (6) corresponds to Equation (5) phase-shifted by  $\pi/2$ . Therefore, Equations (5) and (6) are orthogonal. Now, using Equations (5) and (6), we define the complex first difference:

$$W_{n,t} = w_{n,t} + i \hat{w}_{n,t} = \sum_{k=0}^T c_n(\omega_k) e^{-i\omega_k t} , \quad (7)$$

where  $i$  is an imaginary unit defined by  $i^2 = -1$ , and  $c_n(\omega_k) = a_n(\omega_k) + i b_n(\omega_k)$ . The right hand side of Equation (7) shows that  $W_{n,t}$  rotates in a clockwise direction as time progresses.

The matrix with the components given in Equation (7) is specified as follows:

$$\mathbf{W} = [W_{n,t}] . \quad (8)$$

The complex correlation matrix is defined as follows:

$$\mathbf{C} = \frac{1}{T} \mathbf{W} \mathbf{W}^\dagger , \quad (9)$$

where  $\mathbf{W}^\dagger$  is an adjoint matrix (i.e., transformation and complex conjugate) of  $\mathbf{W}$ . Then,  $\mathbf{C}$  is an Hermitian matrix.

The components of the complex correlation matrix are represented by

$$C_{mn} = \text{Re}(C_{mn}) + i \text{Im}(C_{mn}) \quad (10)$$

$$= |C_{mn}| e^{i \theta_{mn}} , \quad (11)$$

where  $|C_{mn}|$  describes the strength of the linear relationship between the magnitude of the vectors, and  $\theta_{mn}$  represents the correlation in the phase space. In Section 3.5, we will explain how the leading or lagging of the index is derived from  $\theta_{mn}$ .

### 3.2 Random shuffling (RS) and rotational random shuffling (RSS)

We can create a completely random complex correlation matrix by constructing the following randomly shuffle:

$$w_{n,t} \rightarrow w_{n,\text{rand}[1,T]} , \quad (12)$$

where  $\text{rand}[1, T]$  means a random integer from 1 to  $T$  without duplication. We call this manipulation random shuffling (RS). The utterly random complex correlation matrix breaks both the autocorrelation and the cross-correlation.

Many financial and economic time series feature autocorrelation. Therefore, developing a method that preserves the autocorrelation but randomizes cross-correlation is helpful. Iyetomi *et al.* (2011a,b) developed the RRS method to construct such a complex correlation matrix (Souma, 2021). In RRS, we shuffle the empirical time-series data rotationally in the time direction and impose the following periodic boundary condition:

$$w_{n,t} \rightarrow w_{n,\text{mod}[t+\tau,T]} , \quad (13)$$

where  $\tau \in [0, T - 1]$  is a pseudo-random integer that is different for each  $n$ . Therefore, we can construct an RRS complex correlation matrix. However, we must note that we break the autocorrelation at the place where we impose a periodic boundary condition.

### 3.3 Decomposition of the complex correlation matrix

The PCA for the complex correlation matrix  $\mathbf{C}$  derives eigenvalue  $\lambda_j$  and corresponding eigenvector  $\mathbf{v}_j$ , where  $j$  represents the ranking of the eigenvalues and corresponding eigenvectors. Thus, if we can obtain the number of principal components  $n_p$  by applying PCA, we can decompose the complex correlation matrix into its meaningful and noisy parts as follows:

$$\mathbf{C} = \sum_{j=1}^N \lambda_j \mathbf{v}_j \mathbf{v}_j^\dagger = \sum_{j=1}^{n_p} \lambda_j \mathbf{v}_j \mathbf{v}_j^\dagger + \sum_{j=n_p+1}^N \lambda_j \mathbf{v}_j \mathbf{v}_j^\dagger = \mathbf{P} + \mathbf{R} , \quad (14)$$

where  $\mathbf{v}_j^\dagger$  is the adjoint vector (i.e., transformation and complex conjugate) of  $\mathbf{v}_j$ . In Equation (14),  $\mathbf{P}$  and  $\mathbf{R}$  are the principal and noisy parts of the complex correlation matrix, respectively. Therefore, it is reasonable to investigate  $\mathbf{P}$  for revealing the properties of the correlation between the indices.

### 3.4 Mode signal

A mode signal  $\mathbf{I}_j$  is a vector with the number of components equal to the length of time series  $T$  and defined by the product of  $\mathbf{v}_j$  and  $\mathbf{W}$  as follows:

$$\mathbf{I}_j = \mathbf{v}_j^\dagger \mathbf{W} , \quad (15)$$

where  $\mathbf{v}_j^\dagger$  is the adjoint vector (i.e., transformation and complex conjugate) of  $\mathbf{v}_j$ . The mode signal is a valuable tool for detecting the sympathetic structure of the time series.

### 3.5 Correlation network and Helmholtz-Hodge (HH) decomposition

As previously stated, it is reasonable to investigate  $\mathbf{P}$  to reveal the characteristics of the correlation between the indices. The elements of  $\mathbf{P}$  are written as follows:

$$P_{mn} = |P_{mn}| e^{i\theta_{mn}} , \quad (16)$$

where  $\arg(P_{mn}) := \theta_{mn} \in [-\pi, \pi)$ . Generally,  $P_{mn} \neq 0$ . Therefore, the network constructed from  $\mathbf{P}$  is a fully connected complete graph in which complex numbers give the weights of the links. However, it is natural to expect the characteristics of the correlation to be found in the large  $|P_{mn}|$ . Therefore, we set a lower bound (i.e.,  $|P_{mn}| > P_{\min}$ ). If the value of  $P_{\min}$  is too large, the obtained network becomes disconnected. Thus, we

must keep the value of  $P_{\min.}$  in an appropriate range. We define the constrained principal correlation matrix as follows:

$$\tilde{\mathbf{P}} := \mathbf{P} \quad \text{with} \quad |P_{mn}| > P_{\min.} . \quad (17)$$

We expect that the network constructed from Equation (17) will be the backbone of the correlation network.

The Helmholtz-Hodge (HH) decomposition aims to clarify the leading and lagging relationships between indices. In the HH decomposition,  $\theta_{mn}$  represents the flow from index  $m$  to index  $n$  and decomposes  $\theta_{mn}$  into two parts as follows:

$$\theta_{mn} = \theta_{mn}^{(c)} + \theta_{mn}^{(g)} , \quad (18)$$

where  $\theta_{mn}^{(c)}$  corresponds to the circular flow defined as follows:

$$\sum_{n=1}^N \theta_{mn}^{(c)} = 0 . \quad (19)$$

Meanwhile,  $\theta_{mn}^{(g)}$  corresponds to the gradient flow defined as follows:

$$\theta_{mn}^{(g)} = \gamma_{mn} (\phi_m - \phi_n) , \quad (20)$$

where  $\phi_n$  is the HH potential and assigns the leading and lagging relationships to the indices. Here,  $\gamma_{mn}$  is an adjacency matrix given by:

$$\gamma_{mn} = \begin{cases} 1 & \text{If } \theta_{mn} \neq 0 \\ 0 & \text{Otherwise} \end{cases} . \quad (21)$$

Using Equation (20), we can rewrite Equation (19) as follows:

$$\sum_{n=1}^N [\theta_{mn} - \gamma_{mn} (\phi_m - \phi_n)] = 0 . \quad (22)$$

Thus, we obtain  $\phi_n$  by solving Equation (22).

## 4 Results

We apply the CHPCA and the HH methodologies described in Section 3 to the 16 EPU and 19 GPR indices from January 1997 to December 2024 to understand the policy effects and geopolitical influences globally. The results show that the Russian-Ukrainian conflict, which started in February 2022, created significant geopolitical risks and economic policy uncertainties for the rest of the world. The economic impact included increased energy prices, food shortages, inflation, and supply chain disruptions. The Russian invasion of Ukraine was one of the most significant events in the sample period, contributing to increased geopolitical crisis and economic

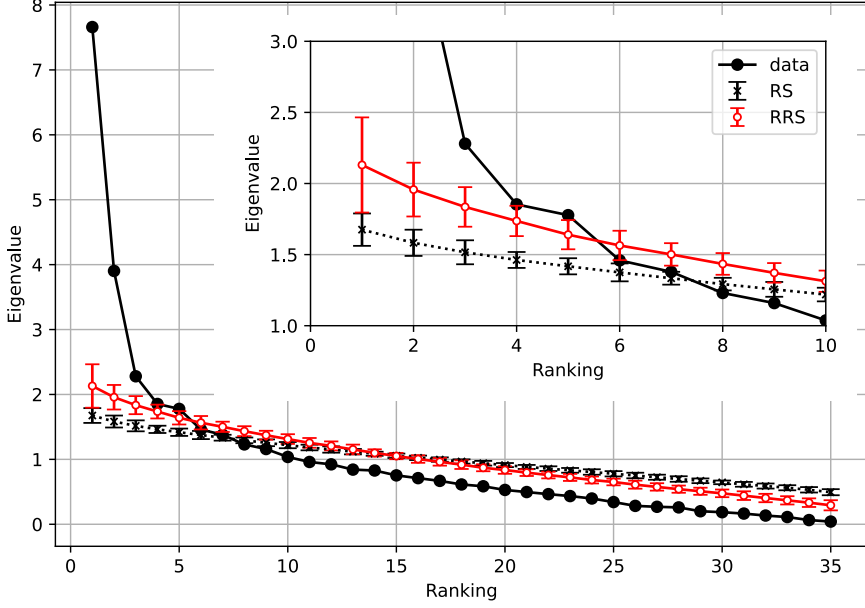


Figure 2: Scree graph of the Complex Correlation Matrix (filled black circles), Randomly Shuffled Complex Correlation Matrix (black crosses), and Rotationally Randomly Shuffled Complex Correlation Matrix (red open circles) for all eigenvalues. This figure shows that the first to fourth eigenvalues are principal components; therefore,  $n_p = 4$ .

uncertainty. Other notable destabilizing events include the September 11, 2001, terrorist attacks on New York City and the U.S.-led invasion of Afghanistan right after the attacks, the Brexit referendum in June 2016, the Covid-19 pandemic and lockdowns starting in March 2020, and the Israeli-Palestinian conflict starting with the Hamas attack on Israel in October 2023.

#### 4.1 Complex Correlation Matrix and Significant Eigenvalues

Figure 2 shows the scree graph for all eigenvalues, and the inset of this figure depicts the zoom-up of the distribution of eigenvalues in the range  $1 \leq j \leq 10$ . In this figure, on the x-axis is the rank of the eigenvalue  $j$ , and on the y-axis is the magnitude of the eigenvalue  $\lambda_j$ . The filled black circles connected by the black line correspond to the distribution of the eigenvalues derived from the complex correlation matrix constructed from the data. The black crosses with absolute error bars connected by the black line represent the distribution of the eigenvalues derived from the randomly shuffled (RS) complex correlation matrix. The red open circles with absolute error bars connected by the red line represent the distribution of the eigenvalues derived from the Rotationally Randomly Shuffled (RRS) complex correlation matrix. By comparing these curves, we confirm that the first four eigenvalues are significant and explain most of the variability in the data; therefore,  $n_p = 4$ .

Figure. 3 shows four principal eigenvectors corresponding to the largest and most significant eigenvalues that describe the different lead-lag relationship characteristics of the EPU's and the GPRs. In these figures, the direction of time progression is clockwise, with the positive real axis as the starting point. Panel  $\mathbf{v}_1$  shows that

components are co-moving, with EPU's leading but with smaller magnitudes compared to the GPRs. Panel  $v_2$  shows that the EPU and the GPU create two distinct groups. The eigenvectors are derived to have the norm equal to one, so there is a degree of freedom in sign. Therefore, it is impossible to say whether the EPU or the GPR is ahead of the other since reversals of this figure's left and right sides are also allowed. The panel  $v_3$  shows a mixture of EPU and GPR components, distributed mainly along the real axis, with the EPU's showing, on average, a smaller radius than the GPRs. The panel  $v_4$  shows a broader distribution of the EPU's and GPRs along both the real and the imaginary axes.

To observe the granularity of the lead-lag relationships among the global EPU's and GPRs, the zoom-up of Figure. 3 is shown in Figure. 4. The radius (absolute value) represents the strength of the eigenvector component, and the phase (argument) determines the lead-lag relationships. As noted in equation (7), each index rotates clockwise over time.

Figure. 4, panel  $v_1$ , corresponding to the largest eigenvalue, shows that the EPU indices lead the GPR indices, which can be interpreted as a global contagion starting with economic policy uncertainty (EPU) and spilling into geopolitical risk (GPR) or political instability. Additionally, since the EPU's exhibit smaller radii than the GPRs, we can infer that even smaller economic policy uncertainties could provoke significant geopolitical instabilities. Among the globally leading indices, we observe the EPU's of China and Russia and the GPRs of Ukraine and Israel.

Figure. 4, panel  $v_2$ , corresponding to the second largest eigenvalue, shows the EPU's and the GPRs distributed in almost opposite directions, with a phase difference of close to  $\pi$ , meaning that the two groups have equal-time negative correlation, which supports the hypothesis that one group follows the other in the phase, revealing the lead-lag relationships able to be detected by the CHPCA methodology. The EPU's radii are larger than the GPRs, meaning that EPU's show higher significance in magnitude. Figure. 4, panel  $v_3$ , corresponding to the third largest eigenvalue, shows mixed distributions of the EPU's and the GPRs, mainly along the real axis, with the EPU's being closer to the origin. The GPRs show larger radii, dominating in significance compared to the EPU's. Figure. 4, panel  $v_4$ , corresponding to the fourth largest eigenvalue, shows EPU and GPR distributions spread out along both the real and imaginary axes, forming approximately two directions, GPR direction with a positive slope, and an EPU direction with a negative slope, with a leading GPR group consisting of Russia and Germany, among others, and a leading EPU group containing India and Japan. The lagging GPR group consists of Israel and Egypt, exhibiting a negative equal-time correlation with the leading GPR group. The lagging EPU group, consisting of China and Russia, shows a negative equal-time correlation with the leading EPU group.

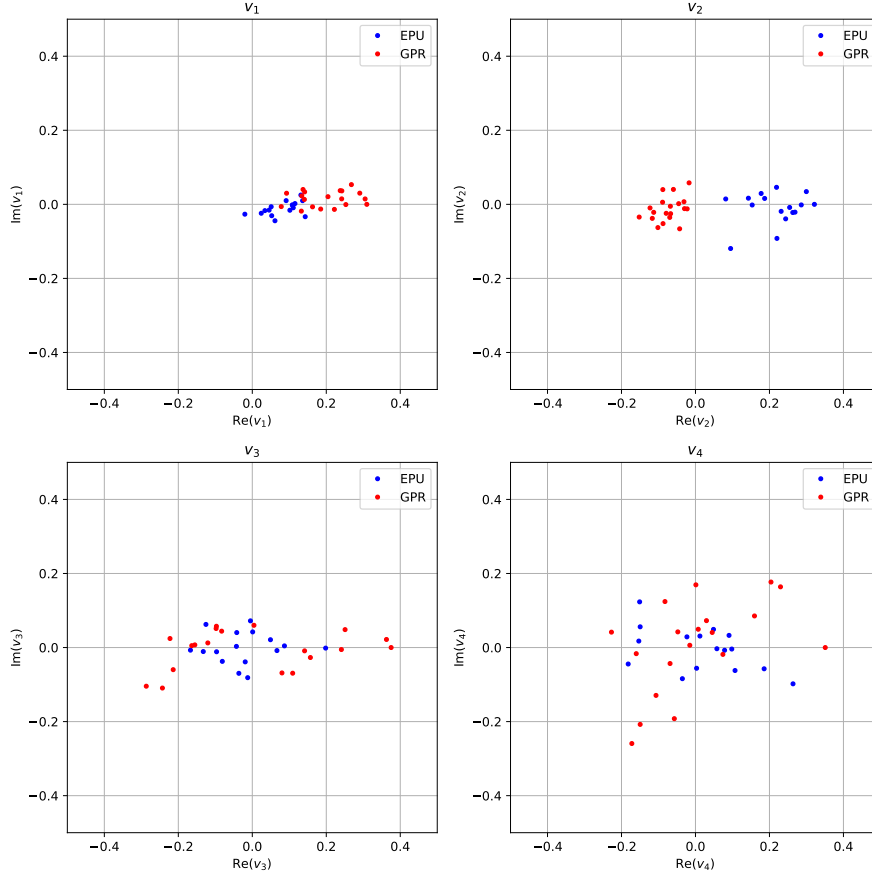


Figure 3: Four principal eigenvectors, i.e.,  $\mathbf{v}_1, \mathbf{v}_2, \mathbf{v}_3, \mathbf{v}_4$ . The blue dots correspond to the EPU indices, and the red dots correspond to the GPR indices. These figures have the same range for the real and the imaginary axes. Panel  $\mathbf{v}_1$  shows that the first eigenvector component distribution is along the positive real axis. This means that the phase difference between each component is small, i.e., components are co-moving, with EPUs leading but with smaller magnitudes compared to GPRs. Panel  $\mathbf{v}_2$  shows that the EPU and the GPU create two distinct groups. In addition, the phase difference between these two groups is close to  $\pi$ , which means that the two groups exhibit equal-time negative correlation. Panel  $\mathbf{v}_3$  shows a mixture of EPU and GPR components, mostly distributed along the real axis, with the EPUs showing, on average, a smaller radius than the GPRs. Panel  $\mathbf{v}_4$  shows a broader distribution of the EPUs and GPRs along both the real and the imaginary axes, with similar magnitudes, and leading and lagging GPR and EPU groups, moving in the following fashion: The leading GPR group is followed by the leading EPU group, then followed by the lagging GPR group, and finally followed by the EPU lagging group.

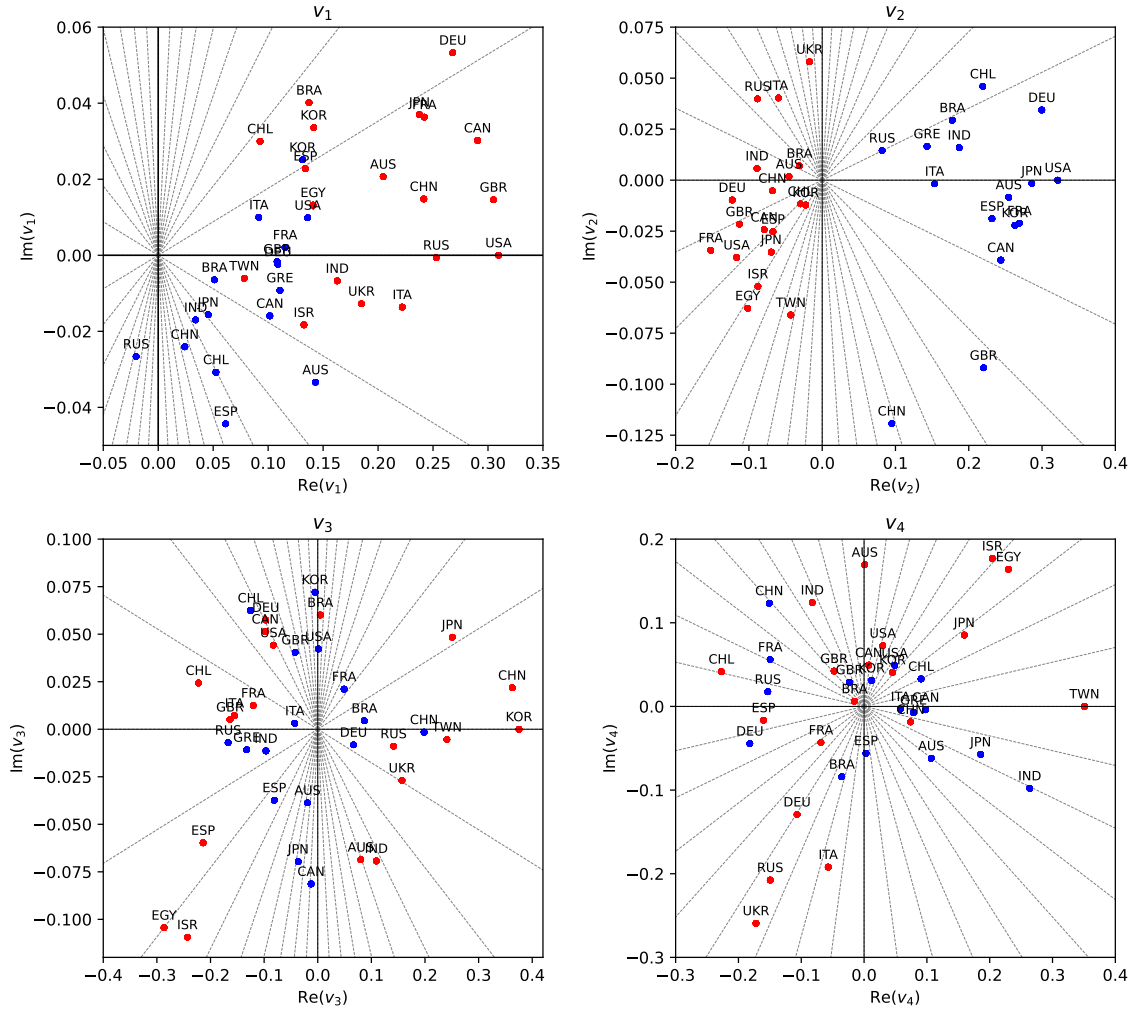


Figure 4: The zoom-up of four principal eigenvectors, i.e.,  $v_1, v_2, v_3, v_4$ . The dotted lines indicate the declination in 10-degree increments. Panel  $v_1$  shows that the EPU indexes have large negative arguments compared to the GPR indexes. This means that the EPU leads the GPR overall. On the other hand, the GPR indexes have larger absolute values (radii) than the EPU indexes. This means that the GPR's impact is stronger than the EPU's. Panel  $v_2$  shows an equal-time negative correlation between the GPRs and the EPUs, with the EPUs dominating in significance, shown by the larger radii than the GPRs. The panel of  $v_3$  shows a mixed distribution of the GPRs and the EPUs mostly along the real axis, with GPRs exhibiting larger radii, and hence higher significance, while the panel of  $v_4$  shows a mixed distribution of the GPRs and the EPUs along both the real and the imaginary axes.

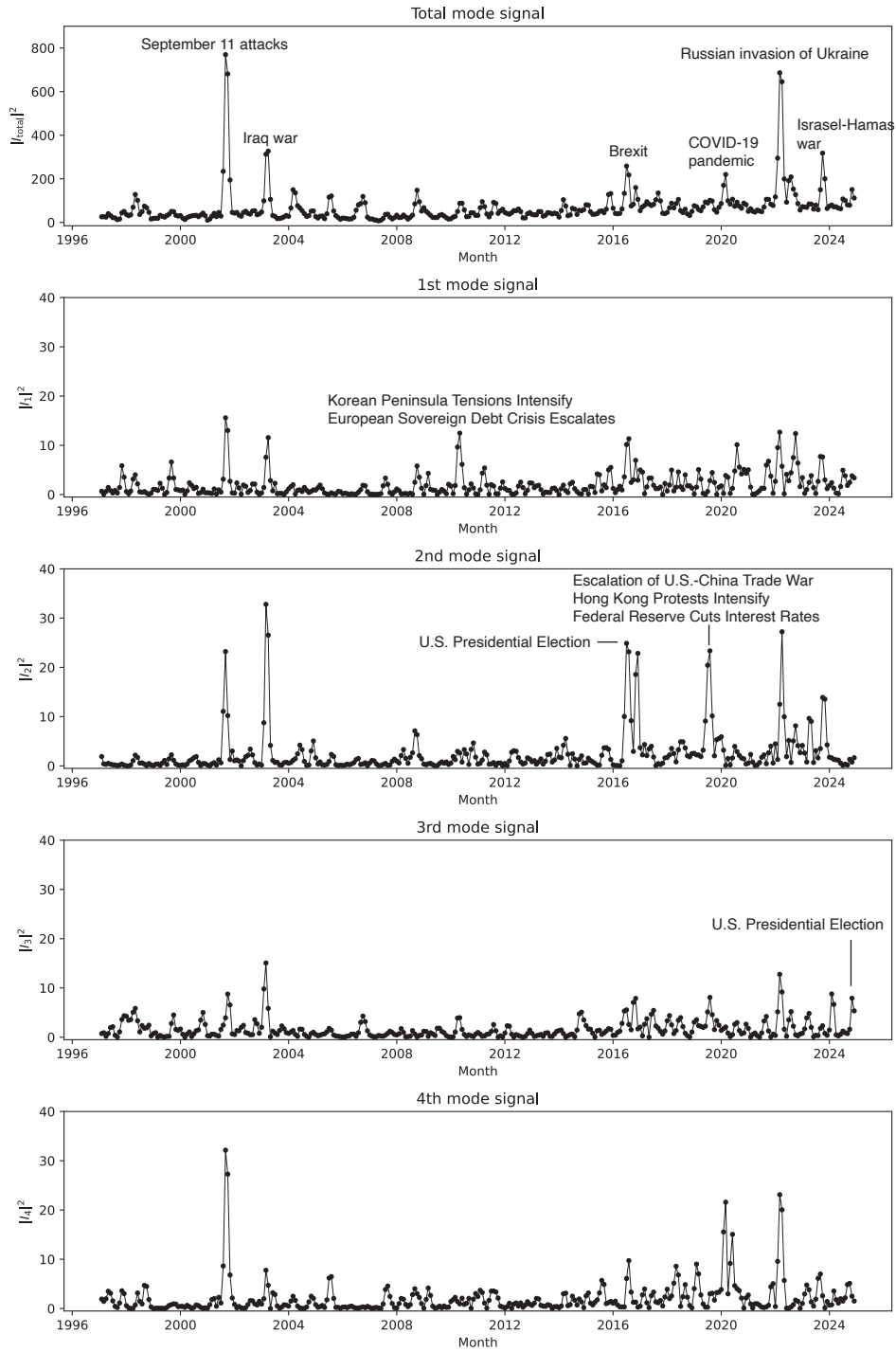


Figure 5: The square value of the total mode signal and the individual mode signals corresponding to the four largest eigenvalues. We identify significant events that dominated between 1997 and 2024 as measured by the EPU and GPR indices for the total mode signal and the individual four mode signals.

## 4.2 Mode signals

We study the mode signals to extract the main events contributing to the EPU and GPR global index dynamics. In addition to the total mode signal, defined by

$$|I_{\text{total},t}|^2 = \sum_{j=1}^N |I_{j,t}|^2, \quad (23)$$

we also investigate the mode signals related to the first four eigenvalues. Eigenmodes related to the largest eigenvalues are key to uncovering important lead-lag relationships among the EPUs and GPRs. This is the case because when the time series is expanded in terms of the eigenvectors, the mode signals' mean strength is proportional to the square root of the corresponding eigenvalues. In Figure 5, we show the squared values of the total mode signal followed by the decomposition of the mode signal to 1st, 2nd, 3rd, and 4th mode signals corresponding to the largest four eigenvalues. We show time on the x-axis and the squared mode signal values on the y-axis.

In the total mode signal, we observe the events that dominate overall during the 28-year period of 1997-2024, including the September 11th terrorist attacks on the U.S., the Iraq war, the Brexit aftermath, the COVID-19 pandemic, the Russian invasion of Ukraine, and the Israeli-Hamas war. In the first mode signal, we additionally identify events such as the intensifying Korean Peninsula tensions and the European Sovereign Debt Crisis in 2010. In the second mode signal, events that dominate the EPU and GPR landscape include the U.S. Presidential election in 2016 and the escalation of the U.S.-China trade war. In the third eigenmode, a newly identified event not observed before is the U.S. Presidential election of 2024, while the other peaks have already been identified in the earlier mode signals. Finally, in the fourth mode signal, we see the effects of earlier detected events such as the 9/11 terrorist attacks, COVID-19, and the Russian invasion of Ukraine.

The top 10 peaks in the total mode signal are summarized in Table 1.

## 4.3 Helmholtz-Hodge Potential Network

Using the four largest eigenvalues,  $n_p = 4$ , we obtain  $\mathbf{P}$  or the principal part of the complex correlation matrix, from Equation (14). The green dots represent the GPR-EPU relationships, the blue dots represent the EPU-EPU relationships, and the red dots represent the GPR-GPR relationships. By using  $P_{\text{min.}} = 0.20$ , calculated from the simulation of the random matrix, we represent the most influential elements of the principal part of the complex correlation matrix  $\tilde{\mathbf{P}}$  as

$$\tilde{P}_{mn} = |\tilde{P}_{mn}| e^{i\tilde{\theta}_{mn}}. \quad (24)$$

We obtain two types of correlation matrices from  $\tilde{\mathbf{P}}$ . One is the matrix constructed from the absolute value of the components,  $|\tilde{P}_{mn}|$ , and the other is constructed from the arguments  $\tilde{\theta}_{mn}$ . The network shown in Figure 7

Table 1: Top 10 event in the sum of square value of total mode signals  $|I_{\text{total}}|^2$ .

| Peak ranking | Month   | Event  |
|--------------|---------|--|
| 1            | 2001-09 | September 11th, 2001 terrorist attacks on New York City and the Pentagon                                   |
| 2            | 2022-03 | Russian airstrike on the Mariupol Theater, intensifying the Russian-Ukraine conflict                       |
| 3            | 2001-10 | U.S. invasion of Afghanistan as a response to the 9/11 terrorist attacks                                   |
| 4            | 2022-04 | The International Monetary Fund issues a warning of growing economic risks due to the Russia-Ukraine war   |
| 5            | 2003-04 | U.S. forces captured Baghdad on April 9, 2003, effectively ending Saddam Hussein's 24-year rule            |
| 6            | 2023-10 | Hamas launched a large-scale attack on Israel, firing over 3,500 rockets and infiltrating southern regions |
| 8            | 2003-03 | The United States, along with coalition forces, initiated military operations against Iraq                 |
| 9            | 2022-02 | Russian invasion of Ukraine on February 24th, 2022   |
| 10           | 2016-07 | Aftermath, following the UK's June 23, 2016, referendum to leave the European Union                        |

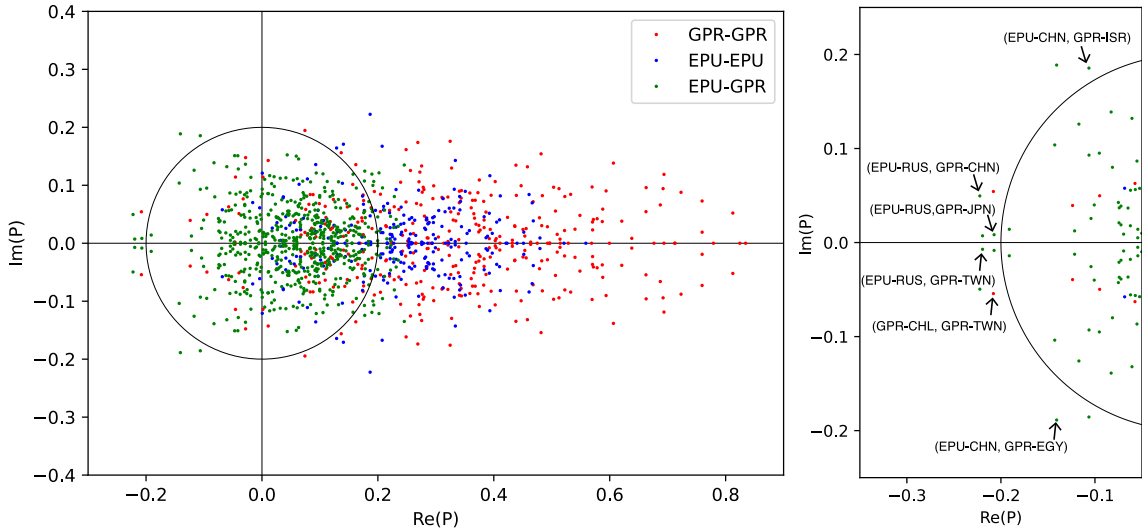


Figure 6: Left Panel: Distribution of the elements of  $\mathbf{P}$  defined by equation (14) and  $\tilde{\mathbf{P}}$  defined by equation (17) with  $P_{\min.} = 0.20$ . Since  $\mathbf{P}$  and  $\tilde{\mathbf{P}}$  are Hermitian matrices, the distribution of the elements is symmetrical on the horizontal axis. The green dots represent the GPR-EPU relationships, the blue dots represent the EPU-EPU relationships, and the red dots represent the GPR-GPR relationships. The points in the circle are random or insignificant, while the points outside are significant. Right Panel: Zoom in on the EPU-GPR relationships corresponding to the negative correlations dominated by the EPU index of Russia's negative correlation with the GPRs of Taiwan, Japan, and China, as well as by the negative correlations of the EPU index of China's negative correlation with the GPRs of Egypt and Israel.

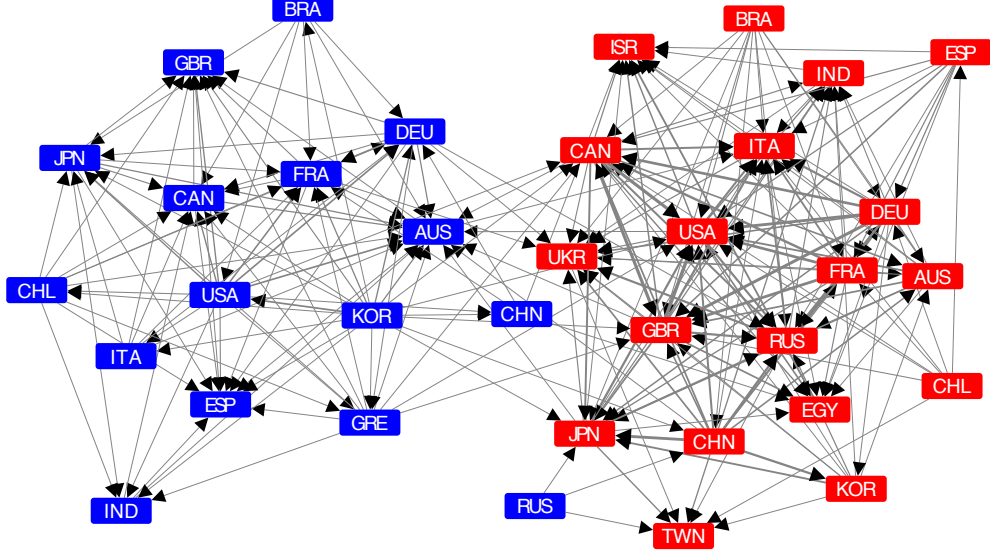


Figure 7: The Correlation network of the EPU and GPRs from February 1997 to December 2024, obtained by using the argument  $\tilde{\theta}_{mn}$ . The directed links represent the HH potential, and the link weights represent the absolute value,  $|\tilde{P}_{mn}|$ .

is constructed using  $\tilde{\theta}_{mn}$ , with the direction of the links representing the HH potential as obtained by solving Equation (22), while the weight of links is obtained by  $|\tilde{P}_{mn}|$ .

Table. 2 gives the summary of the incoming degree  $k_{in}$  and the outgoing degree  $k_{out}$  for each country derived from the network shown in Figure. 7. In this table,  $w_{in}$  represent  $w_{out}$  the sum of the weights defined by

$$w_{in,m} = \sum_{n \in in(m)} |\tilde{P}_{mn}|, \quad w_{out,m} = \sum_{n \in out(m)} |\tilde{P}_{mn}|. \quad (25)$$

Table 2 reveals that the countries with the highest incoming EPU degrees as well as the highest incoming link total weights are Great Britain, Australia, and Canada, meaning that these countries' EPU have been the most influenced by other countries' EPU and GPRs. The United States and South Korea have the highest outgoing degrees and outgoing link weights, meaning that these countries have influenced most other countries' EPU and GPRs. Countries with the highest incoming GPR degrees are Italy and Ukraine. At the same time, we observe the highest GPR incoming link weights for the United States and Russia, meaning that these countries have been influenced the most by other countries' GPR and EPU indices. Finally, the leaders in the number of outgoing GPR links and the highest outgoing GPR link weights are Germany and China, meaning that they have influenced the EPU and GPRs of other countries to a great extent between 1997 and 2024.

Figure 8 shows the HH potential for EPU and GPRs. The x-axis corresponds to the HH potential  $\phi_n$  of index  $n$ , and the y-axis corresponds to the index names. The blue bars represent the EPU indices, and the red bars represent the GPR indices. A high  $\phi_n$  value indicates a leading index  $n$ . Therefore, a rightward direction represents a leading property of the index. On the other hand, if the index  $n$  is lagging, the corresponding  $\phi_n$

Table 2: Degrees and sum of the weights for the incoming and outgoing links of the GPR and EPU indices.

| Country<br>Code | EPU      |          |           |           | GPR      |          |           |           |
|-----------------|----------|----------|-----------|-----------|----------|----------|-----------|-----------|
|                 | $k_{in}$ | $w_{in}$ | $k_{out}$ | $w_{out}$ | $k_{in}$ | $w_{in}$ | $k_{out}$ | $w_{out}$ |
| AUS             | 11       | 3.768    | 3         | 0.869     | 11       | 3.361    | 9         | 3.264     |
| BRA             | 1        | 0.225    | 6         | 1.446     | 0        | 0        | 11        | 3.185     |
| CAN             | 13       | 3.66     | 3         | 0.976     | 7        | 3.022    | 11        | 5.354     |
| CHL             | 2        | 0.632    | 9         | 2.317     | 0        | 0        | 8         | 2.276     |
| CHN             | 4        | 0.865    | 4         | 1.006     | 1        | 0.291    | 14        | 6.481     |
| FRA             | 9        | 2.782    | 5         | 1.524     | 5        | 1.977    | 11        | 5.17      |
| DEU             | 6        | 1.938    | 9         | 2.928     | 4        | 1.476    | 13        | 6.374     |
| GRE             | 4        | 0.995    | 10        | 2.322     | 0        | 0        | NA        | NA        |
| IND             | 5        | 1.291    | 3         | 0.78      | 10       | 3.639    | 3         | 0.694     |
| ITA             | 3        | 0.752    | 6         | 1.392     | 13       | 5.196    | 3         | 0.967     |
| JPN             | 9        | 2.443    | 6         | 1.953     | 8        | 3.803    | 9         | 3.214     |
| KOR             | 0        | 0        | 19        | 5.545     | 2        | 0.804    | 9         | 2.902     |
| RUS             | 1        | 0.236    | 3         | 0.655     | 11       | 5.244    | 4         | 1.646     |
| ESP             | 10       | 2.862    | 1         | 0.262     | 1        | 0.284    | 9         | 3.075     |
| GBR             | 13       | 3.808    | 0         | 0         | 9        | 4.464    | 9         | 4.371     |
| USA             | 4        | 1.196    | 13        | 4.643     | 11       | 5.91     | 7         | 3.031     |
| EGY             | 1        | 0.235    | NA        | NA        | 9        | 3.155    | 1         | 0.514     |
| ISR             | 1        | 0.214    | NA        | NA        | 11       | 3.584    | 0         | 0         |
| TWN             | 1        | 0.22     | NA        | NA        | 6        | 1.781    | 0         | 0         |
| UKR             | 2        | 0.497    | NA        | NA        | 13       | 4.735    | 1         | 0.208     |

is low. Hence, the leftward direction represents a lagging index. Thus, in this figure, we observe that the most significant leading index is the EPU for Russia, and the most lagging index is the GPR for Taiwan.

## 5 Discussion

This study investigates the complex global correlations between the 16 EPU and 19 GPR indices. We explore these 35 monthly time series for the 28 years from January 1997 to December 2024. We apply a novel CHPCA methodology to extract significant lead-lag relationships between the EPUs and GPRs and to understand the significant influences of specific countries' geopolitical risk or economic policy uncertainties on others.

We identified four significant eigenvalues from the complex correlation matrix and studied each related eigenmode separately to identify significant events dominating the EPU-GPR landscape during the last 28 years. The analysis of the first principal eigenvector components shows that while, in general, the EPUs show leading characteristics, they exhibit smaller magnitudes compared to the GPRs. Overall, all indices in the first largest eigenvector are distributed along the real axis with a small phase difference, signifying a co-movement of the EPU and GPR indices. The second largest principal eigenvector components reveal the presence of an equal-time negative correlation between the EPUs and GPRs. In contrast, the third and fourth principal eigenvector components show mixed distributions where the EPUs are closer to the origin or have smaller radii than the GPRs, which show greater significance. In the leading pack of the first principal eigenvector components, we

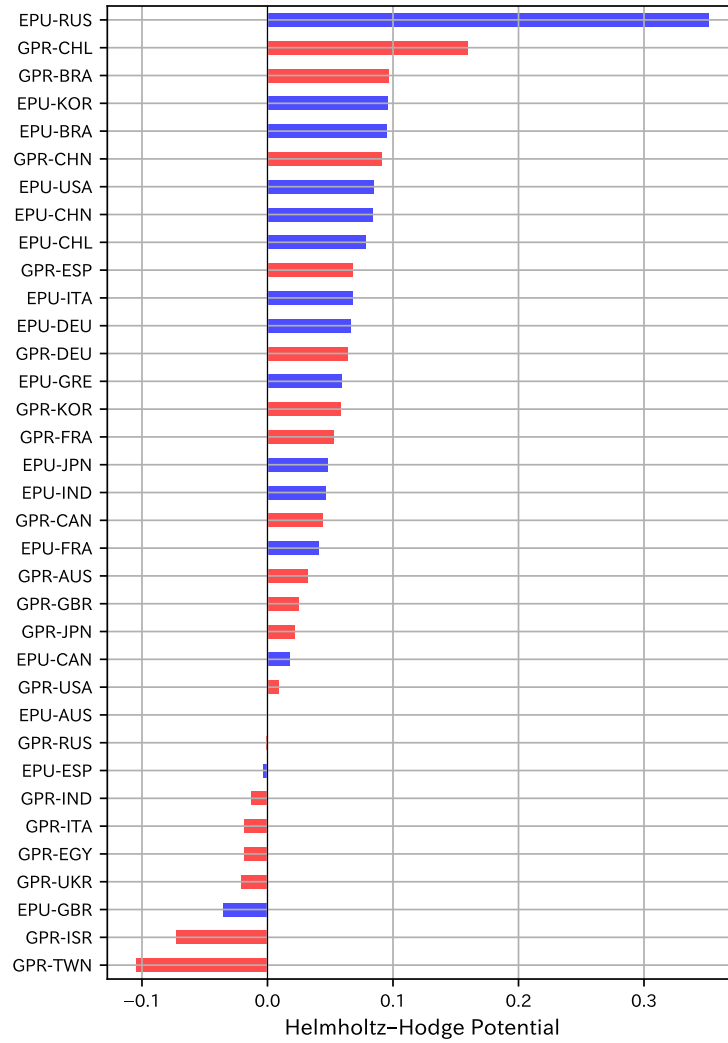


Figure 8: Helmholtz-Hodge potential from January 1997 to December 2024. The rightward direction corresponds to the leading role of the index, showing that the EPU of Russia is the most significant leading index. On the other hand, the leftward direction corresponds to the lagging indices, showing that the index that lags the most is Taiwan's GPR.

see the EPU of Russia and China and the GPRs of Israel and Ukraine, followed by larger-in-magnitude GPRs of the United States, Great Britain, Canada, Germany, Japan, Russia, and China.

The total mode signal reveals the most significant events, such as the 9/11 terrorist attack on New York City and the Pentagon in 2001 and the Russian invasion of Ukraine in February 2022, which had significant economic impacts, including increased inflation and high energy prices, as well as supply chain disruptions. Other events include the Iraq war in 2003, the Brexit aftermath in 2016, the COVID-19 pandemic in 2020, and the Israeli-Hamas war in 2023. In the analysis of the eigenmodes corresponding to the largest four principal components, we identify additional significant events, including the Korean Peninsula tensions and the European Sovereign Debt crisis in 2010, the U.S. Presidential elections of 2016 and 2024, and the escalation of the U.S.-China trade war.

The principal component of the complex correlation matrix, constructed by using the four largest eigenvalues, reveals that most of the EPU and GPRs show co-movement and significant positive correlations with larger values in the GPR-GPR relations followed by the EPU-EPU relation. We observe an exception of six negative correlations mostly related to the EPU of Russia's negative correlation with the GPRs of Taiwan, Japan, and China, and the EPU of China's negative correlations with the GPRs of Egypt and Israel. The majority of the EPU-GPR relations, however, fall in the non-significant or random realm. The HH potential shows that the most influential, leading index is the EPU of Russia, followed by the GPR indices of Chile and Brazil. The most lagging index is the GPR of Taiwan.

We have used the HH potential to construct the directed complex correlation network and have found that by investigating the incoming and outgoing network links and the link weights, we can identify the indices that show the highest effect by other countries as well as indices that affect most of the others. Great Britain, Canada, and Australia's EPU indices have been the most influenced by other countries, and the EPU of the United States and South Korea have been the biggest influencers of others. The GPRs of Italy and Ukraine have been the most influenced by other countries, and the biggest GPR influencers are Germany and China.

The limitations of this study include differences in the number of data sources for the EPU and GPR indices for different countries, and a low (monthly) resolution of the EPU and GPR indices.

The contribution of this study is three-fold: 1. Once specific economic policy uncertainty measured by the EPU and geopolitical tensions measured by the GPRs have been documented to impact other countries significantly, these relationships can be used as early warning signals of possible future impacts and can aid governments and policymakers with making informed decisions. 2. Our findings can be the basis for creating real-time monitoring of EPU and GPRs by creating a financial, economic, and geopolitical observatory, where the existing monthly indices can be complemented with real-time Natural Language Processing (NLP) analysis of real-time news to inform the relevant decision-makers of potential imminent risks timely. 3. The novel CHPCA methodology can be expanded into different economic, financial, and policy applications, including

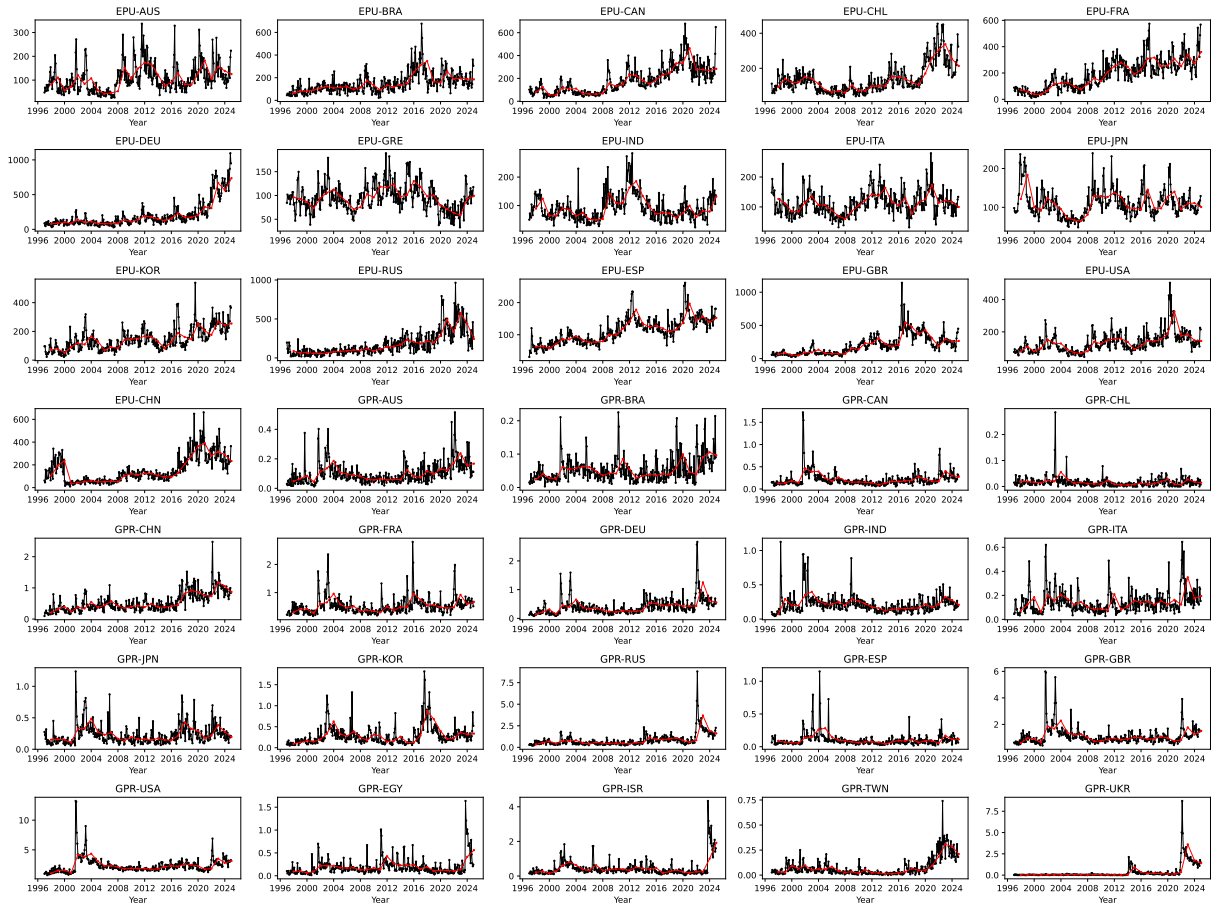


Figure 9: The original time series of EPUs for 16 countries and GPRs for 19 countries. The solid black lines with dots correspond to the original monthly time series. The solid red lines correspond to the annual average normalized by the highest value of each index.

designing state-of-the-art monitoring tools for politicians and governments that can contribute to decisions resulting in improved economic and geopolitical stability.

## Appendix

The original time series of EPUs for 16 countries and GPRs for 19 countries are shown in Figure. 9. The top three rows and the figure on the left in the fourth row show the time series of EPUs. These figures can be broadly divided into two categories: those that show a rightward trend (EPU-BRA, EPU-CAN, EPU-CHL, EPU-FRA, EPU-DEU, EPU-KOR, EPU-RUS, EPU-ESP, EPU-CHN) and those that do not (EPU-AUS, EPU-GRE, EPU-IND, EPU-ITA, EPU-JPN, EPU-GBR, EPU-USA).

The panels after the second panel from the left in row four correspond to GPR. Unlike in the case of the EPUs, a rightward trend does not exist for the GPRs. Instead, sharp peaks exist in many GPRs. There are resemble time series, such as the pair of GPR-RUS and GPR-UKR and the pair of GPR-ISR and GPR-EGP.

## References

- Aoyama, H., Fujiwara, Y., Ikeda, Y., Iyetomi, H., Souma, W. and Yoshikawa, H., *Macro-Econophysics: New Studies on Economic Networks and Synchronization*, 2017 (Cambridge University Press: Cambridge, UK).
- Arai, Y., Yoshikawa, T. and Iyetomi, H., Complex principal component analysis of dynamic correlations in financial markets. In *Intelligent Decision Technologies*, pp. 111–119, 2013, (IOS Press).
- Baker, S.R., Bloom, N. and Davis, S.J., Measuring economic policy uncertainty. *Q. J. Econ.*, 2016, **131**, 1593–1636.
- Balli, F., Balli, H.O., Hasan, M. and Gregory-Allen, R., Geopolitical risk spillovers and its determinants. *Ann. Reg. Sci.*, 2022, **68**, 463–500.
- Balli, F., Uddin, G.S., Mudassar, H. and Yoon, S.M., Cross-country determinants of economic policy uncertainty spillovers. *Econ. Lett.*, 2017, **156**, 179–183.
- Baruník, J. and Křehlík, T., Measuring the frequency dynamics of financial connectedness and systemic risk. *J. Financ. Econom.*, 2018, **16**, 271–296.
- Bernanke, B.S., Irreversibility, uncertainty, and cyclical investment. *Q. J. Econ.*, 1983, **98**, 85–106.
- Bloom, N., The impact of uncertainty shocks. *Econometrica*, 2009, **77**, 623–685.
- Bloom, N., Observations on uncertainty. *Aust. Econ. Rev.*, 2017, **50**, 79–84.
- Caggiano, G., Castelnuovo, E. and Figueres, J.M., Economic policy uncertainty spillovers in booms and busts. *Oxf. Bull. Econ. Stat.*, 2020, **82**, 125–155.
- Caldara, D. and Iacoviello, M., Measuring geopolitical risk. *Am. Econ. Rev.*, 2022, **112**, 1194–1225.
- Castelnuovo, E., Lim, G. and Pellegrino, G., A short review of the recent literature on uncertainty. *Aust. Econ. Rev.*, 2017, **50**, 68–78.
- Diebold, F.X. and Yilmaz, K., Measuring financial asset return and volatility spillovers, with application to global equity markets. *Econ. J.*, 2009, **119**, 158–171.
- Diebold, F.X. and Yilmaz, K., Better to give than to receive: Predictive directional measurement of volatility spillovers. *Int. J. Forecast.*, 2012, **28**, 57–66.
- Diebold, F.X. and Yilmaz, K., On the network topology of variance decompositions: Measuring the connectedness of financial firms. *J. Econom.*, 2014, **182**, 119–134.

- Diebold, F.X. and Yilmaz, K., *Financial and Macroeconomic Connectedness: A Network Approach to Measurement and Monitoring*, 2015 (Oxford University Press: New York, NY).
- EPU, Economic Policy Uncertainty Index. <https://www.policyuncertainty.com>, 2025.
- Horel, J.D., Complex principal component analysis: Theory and examples. *J. Appl. Meteorol. Climatol.*, 1984, **23**, 1660–1673.
- Iyetomi, H., Aoyama, H., Fujiwara, Y., Souma, W., Vodenska, I. and Yoshikawa, H., Relationship between macroeconomic indicators and economic cycles in US. *Scientific reports*, 2020, **10**, 8420.
- Iyetomi, H., Nakayama, Y., Aoyama, H., Fujiwara, Y., Ikeda, Y. and Souma, W., Fluctuation-dissipation theory of input-output interindustrial relations. *Phys. Rev. E*, 2011a, **83**, 016103.
- Iyetomi, H., Nakayama, Y., Yoshikawa, H., Aoyama, H., Fujiwara, Y., Ikeda, Y. and Souma, W., What causes business cycles? Analysis of the Japanese industrial production data. *J. Jpn. Int. Econ.*, 2011b, **25**, 246–272.
- Kang, S.H. and Yoon, S.M., Dynamic connectedness network in economic policy uncertainties. *Appl. Econ. Lett.*, 2019, **26**, 74–78.
- King, M.A. and Wadhvani, S., Transmission of volatility between stock markets. *Rev. Financ. Stud.*, 1990, **3**, 5–33.
- Klößner, S. and Sekkel, R., International spillovers of policy uncertainty. *Econ. Lett.*, 2014, **124**, 508–512.
- Liow, K.H., Liao, W.C. and Huang, Y., Dynamics of international spillovers and interaction: Evidence from financial market stress and economic policy uncertainty. *Econ. Model.*, 2018, **68**, 96–116.
- Marfatia, H., Zhao, W.L. and Ji, Q., Uncovering the global network of economic policy uncertainty. *Res. Int. Bus. Financ.*, 2020, **53**, 101223.
- Rasmusson, E.M., Arkin, P.A., Chen, W.Y. and Jalickee, J.B., Biennial variations in surface temperature over the United States as revealed by singular decomposition. *Mon. Weather Rev.*, 1981, **109**, 587–598.
- Souma, W., Characteristics of principal components in stock price correlation. *Front. Phys.*, 2021, **9**, 1–12.
- Vodenska, I., Aoyama, H., Fujiwara, Y., Iyetomi, H. and Arai, Y., Interdependencies and causalities in coupled financial networks. *PLoS ONE*, 2016, **11**, 1–32.
- Yang, L., Luo, J. and Jiang, Y., Policy uncertainty spillovers and financial risk contagion in the Asia-Pacific network. *Pac-Basin Financ. J.*, 2021, **67**, 101554.